Nanoscale

COMMUNICATION

Synthesis of two-dimensional titanium nitride Ti_4N_3 (MXene)†

Cite this: *Nanoscale*, 2016, **8**, 11385

Received 17th March 2016,
Accepted 9th May 2016

DOI: 10.1039/c6nr02253g

www.rsc.org/nanoscale

Patrick Urbankowski,‡[a] Babak Anasori,‡[a] Taron Makaryan,[a] Dequan Er,[b] Sankalp Kota,[a] Patrick L. Walsh,[a] Mengqiang Zhao,[a] Vivek B. Shenoy,[b] Michel W. Barsoum[a] and Yury Gogotsi*[a]

We report on the synthesis of the first two-dimensional transition metal nitride, Ti_4N_3-based MXene. In contrast to the previously reported MXene synthesis methods – in which selective etching of a MAX phase precursor occurred in aqueous acidic solutions – here a molten fluoride salt is used to etch Al from a Ti_4AlN_3 powder precursor at 550 °C under an argon atmosphere. We further delaminated the resulting MXene to produce few-layered nanosheets and monolayers of $Ti_4N_3T_x$, where T is a surface termination (F, O, or OH). Density functional theory calculations of bare, non-terminated Ti_4N_3 and terminated $Ti_4N_3T_x$ were performed to determine the most energetically stable form of this MXene. Bare and functionalized Ti_4N_3 are predicted to be metallic. Bare Ti_4N_3 is expected to show magnetism, which is significantly reduced in the presence of functional groups.

The family of two-dimensional (2D) materials—solids with high aspect ratios and thicknesses of a few atomic layers—has grown far beyond graphene.[1–4] 2D transition metal carbides and carbonitrides, known as MXenes, are one of the latest additions to this family. Interest in researching the properties of MXenes is still growing.[5–9] MXenes have been produced by selectively etching the A layers from MAX phases.[10–13] The latter are named after their constituent elements: in $M_{n+1}AX_n$, M is an early transition metal, A is a group IIIA or IVA element, X is C and/or N, and n = 1, 2 or 3.[14,15] There are currently over 70 MAX phases known and an even greater amount of solid solutions of these phases.[15–17] These materials have a layered hexagonal crystal structure with the $P6_3/mmc$ symmetry, where M layers are nearly closed packed and X atoms fill the octahedral sites, and adjacent $M_{n+1}X_n$ layers are interleaved with pure A-layers.[18] The M–X bond in MAX phases has a predominantly mixed covalent/metallic character, whereas the M–A bond is metallic,[19] therefore the bonds between the MAX layers cannot be easily broken mechanically.[14] Since the M–A bonds are weaker than the M–X bonds, we have shown that it is possible to selectively etch the A-layers with aqueous solutions containing fluoride ions, such as aqueous hydrofluoric acid (HF),[10] a mixture of lithium fluoride and hydrochloric acid,[20] or with ammonium bifluoride,[21] yielding MXenes.[10,11,14,22] In this process, the Al atoms are removed, and the M–X layers are terminated with O, OH and/or F atoms, producing functionalized MXenes.[14] Functional groups, or terminations, are abbreviated as T in the general formula $M_{n+1}X_nT_x$.

Other methods of selectively removing the A element have also been reported but produced phases that are not MXenes, such as heating the MAX phase under vacuum,[23] immersion in liquid metal,[24] or molten salts,[24,25] or by treatment in anhydrous HF at 55 °C.[26] Etching in molten salts also selectively removes the A atoms, *e.g.* Al in Ti_2AlC[27] and Si in Ti_3SiC_2.[25] In these molten salt etching procedures, however, de-twinning of the $M_{n+1}X_n$ layers occurred, resulting in the formation of a non-stoichiometric Ti–C rock salt structure with partially ordered vacancies.[25,27]

Although treatment in aqueous acidic solutions works well for producing carbide and carbonitride MXenes, for reasons that are not clear they fail to etch out A layers from nitride-based MAX phases.[28,29] For example, treating Ti_4AlN_3 in dilute HF at room temperature (RT) produces nanosheets of Ti_4AlN_3.[28] To date, several MXenes have been synthesized including Ti_3C_2, Ti_2C, Nb_2C, V_2C, Ta_4C_3, Mo_2C, $(Mo_2Ti)C_3$, Zr_3C_2 among others,[11–13,22,30,31] but until now, nitride MXenes have not been reported. The difficulty in producing nitride MXenes may be caused by two factors. The calculated cohesive energies of $Ti_{n+1}N_n$ are less than those of $Ti_{n+1}C_n$, whereas the formation energies of $Ti_{n+1}N_n$ from $Ti_{n+1}AlN_n$ are higher than those of $Ti_{n+1}C_n$ from $Ti_{n+1}AlC_n$.[32] Lower cohesive energy implies lower stability of the structure of $Ti_{n+1}N_n$, whereas the higher formation energy of $Ti_{n+1}N_n$ implies that the Al atoms in $Ti_{n+1}AlN_n$ are more strongly bonded, therefore requiring

[a]*A.J. Drexel Nanomaterials Institute and Department of Materials Science & Engineering, Drexel University, Philadelphia, PA 19104, USA. E-mail: gogotsi@drexel.edu; Fax: +1-215-895-1934; Tel: +1-215-895-6446*

[b]*Department of Materials Science and Engineering, University of Pennsylvania, Philadelphia, Pennsylvania 19104, USA*

†Electronic supplementary information (ESI) available. See DOI: 10.1039/c6nr02253g

‡These authors contributed equally to this work.

more energy for their extraction.[14] Another possibility of why nitride MXenes have previously not been produced is that the lower stability of $Ti_{n+1}N_n$ caused it to dissolve in aqueous HF solution, the etchant used to chemically exfoliate $Ti_{n+1}AlN_n$ to produce $Ti_{n+1}N_n$.[14]

Nitride MXenes have several potential advantages over their carbide counterparts. Transition metal nitrides are known to have higher electronic conductivities than carbides,[33] they are therefore suitable candidates for electrodes in electrochemical capacitors.[34] TiN is known as a promising plasmonic material, suggesting that nitride MXenes also offer better performance for transformation optics and metamaterial devices.[35] Based on the computational results, it has been predicted that Ti_4N_3 with O, F, or OH functional surface groups has a higher density of states, DOS, at the Fermi level, $N(E_F)$, than either Ti_4C_3 or Ti_3C_2 with the same terminations.[36] Furthermore, $N(E_F)$ increases with increasing n in $Ti_{n+1}X_n$ for carbides and nitrides covered with functional groups.[36] The increased electron count due to the presence of N atoms may outweigh the withdrawal of electrons by surface groups, thereby further preserving a functionalized nitride MXene's metallic character.[14]

This work investigated the heating of Ti_4AlN_3 in a molten salt under an argon (Ar) atmosphere in order to synthesize $Ti_4N_3T_x$. X-ray diffraction (XRD), Raman spectroscopy and transmission electron microscopy (TEM) confirmed the selective etching of Al atoms from Ti_4AlN_3 and the preservation of the Ti–N bonds in a layered hexagonal Ti_4N_3 structure as a result of this procedure. The method herein reported has the potential to be applied to other MAX phases to produce their corresponding MXenes. Density functional theory (DFT) calculations were also used to analyze the stability, and the electronic and magnetic properties of this MXene.

Details of Ti_4AlN_3 and $Ti_4N_3T_x$ synthesis and molten salt treatment can be found in the ESI.† In short, Ti_4AlN_3 powder was mixed with a fluoride salt mixture in a 1 : 1 mass ratio. The fluoride salt mixture comprised of 59 wt% of potassium fluoride (KF), 29 wt% of lithium fluoride (LiF), and 12 wt% of sodium fluoride (NaF) and corresponds to the ternary eutectic composition in this salt system. The mixture of Ti_4AlN_3 and fluoride salt was heated at 550 °C for 30 min, with a heating rate of 10 °C min^{-1} from room temperature under Ar flow in an alumina crucible. The synthesis process is schematically shown in Scheme 1.

The XRD pattern of the molten salt treated Ti_4AlN_3 – before dissolving the salt – shows evidence for five different fluoride phases (Fig. 1a), all of which contain Al, revealing the depletion of Al from Ti_4AlN_3 due to its reaction with the molten salt mixture (compare the bottom and middle XRD patterns in Fig. 1). The absence of Ti-containing fluorides in the XRD pattern confirms the selective etching of Al. The presence of Ti_4AlN_3 peaks shows that there are non-etched MAX phase particles remaining after the salt treatment. In addition, two new peaks appear near the original Ti_4AlN_3 (002) peak, which is at ~7.6°. The first peak, around ~6.3°, is quite broad (left dashed line in Fig. 1a and S1†), and possibly due to the (002) peak of a layered structure, with a *c*-lattice parameter (*c*-LP) of 27 Å, possibly of $Ti_4N_3T_x$. One can argue that this broad peak comes from diffuse scattering. However, the appearance of another broad peak at 12.7° (second dashed line in Fig. 1a and S1†), which can be the (004) peak, suggests that the ~6.3° peak is not from diffuse scattering. These two peaks are the first evidence for $Ti_4N_3T_x$ formation, which are discussed further below. We noted the presence of another peak at 8.9° 2θ – marked with a dotted line and a question mark in Fig. 1a – in both the untreated and the molten salt treated Ti_4AlN_3. In the MAX phases, the M_3AX_2 phases have a peak at around 9° 2θ. However, to our knowledge, Ti_3AlN_2 does not exist. Further studies are needed to understand the nature of this peak.

To dissolve the Al-containing fluorides, diluted sulfuric acid (H_2SO_4) was used. The etching products were subsequently removed by washing with deionized (DI) water followed by centrifugation and decanting the supernatant fluid

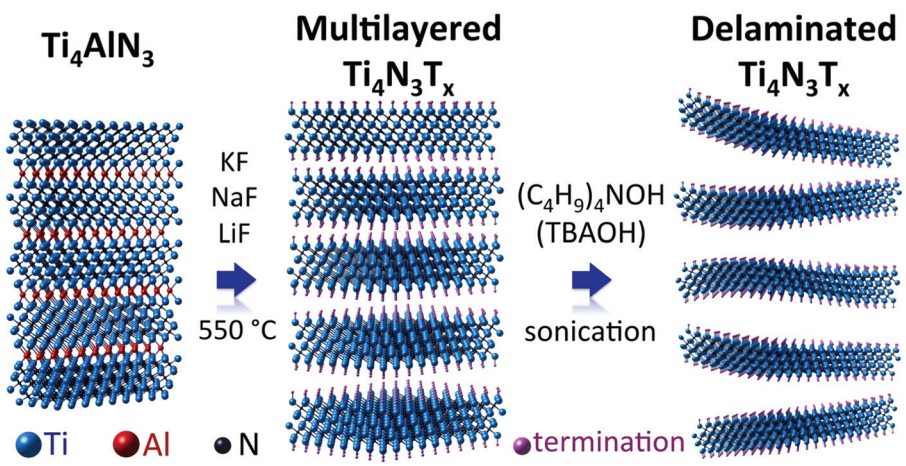

Scheme 1 Schematic illustration of the synthesis of $Ti_4N_3T_x$ by molten salt treatment of Ti_4AlN_3 at 550 °C under Ar, followed by delamination of the multilayered MXene by TBAOH.

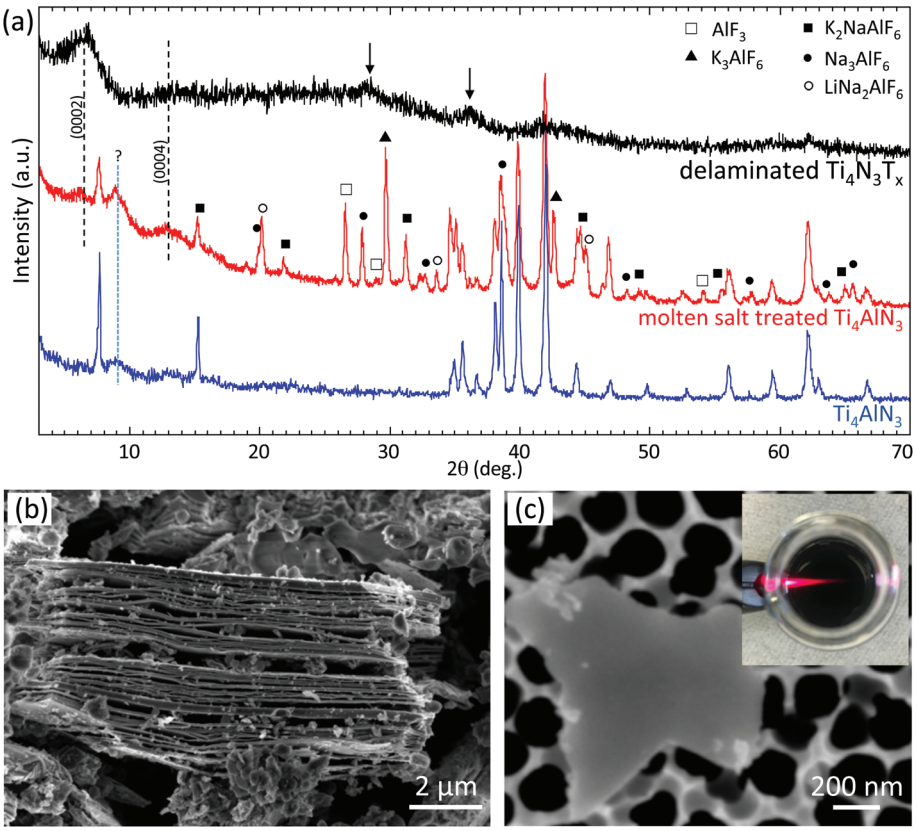

Fig. 1 (a) XRD patterns of Ti_4AlN_3, molten salt treated Ti_4AlN_3, and delaminated $Ti_4N_3T_x$. All peaks for the molten salt treated Ti_4AlN_3 are identified, all the fluoride salt peaks are marked and the Ti_4AlN_3 peaks are not marked, which match the bottom (Ti_4AlN_3) pattern. Peaks possibly corresponding to rutile (TiO_2) are marked with arrows in the top (d-$Ti_4N_3T_x$) pattern. (b) SEM image of molten salt treated Ti_4AlN_3 at 550 °C for 0.5 h under Ar flow. (c) SEM image of few-layered $Ti_4N_3T_x$ particle on an alumina filter substrate. The inset in (c) shows the Tyndall effect for delaminated flakes dispersed in water.

until the pH was at least 6. After the last decanting step, the sediment was filtered on a polypropylene membrane. Its XRD pattern (Fig. S1 in the ESI†) shows that almost all the fluoride salts are removed and that the resulting powder contains $Ti_4N_3T_x$ and unetched Ti_4AlN_3.

To delaminate the multilayered $Ti_4N_3T_x$ MXene into few- and single-layered flakes and remove the non-etched Ti_4AlN_3, the powder was mixed with tetrabutylammonium hydroxide (TBAOH) (see the ESI†).[37] The TBAOH was then removed by washing with DI water and then centrifuged and decanted. DI water was added to the remaining powder, probe sonicated for 0.5 h and centrifuged at 5000 rpm for 0.25 h. The supernatant suspension was then filtered to collect the smaller delaminated $Ti_4N_3T_x$ flakes. These flakes are henceforth referred to as delaminated $Ti_4N_3T_x$ or d-$Ti_4N_3T_x$.

Typical of all the MAX to MXene transformations, the (00l) peaks broaden and shift to lower angles as a result of an increase in the *c*-LP. As discussed earlier, the XRD pattern of Ti_4AlN_3 after molten salt treatment shows a quite weak broad peak at 6.3°. A stronger broad peak, at a similar 2θ, is the strongest peak in the d-$Ti_4N_3T_x$ pattern (top pattern in Fig. 1a), showing a shift of the (002) peak from 2θ = 7.6° to ~6.3°, corresponding to the *c*-LPs of 23 Å to ~28 Å, for Ti_4AlN_3 and $Ti_4N_3T_x$, respectively (Fig. 1a). This increase can be due to: (i) intercalation of ions during molten salt treatment, which was also observed in its XRD pattern (middle pattern Fig. 1a) and/or, (ii) water intercalation in between the layers after delamination in an aqueous solution. This increase is smaller than those of the previously reported M_4X_3 MXenes such as Nb_4C_3,[38] etched in aqueous HF, that resulted in a *c*-LP of 31 Å. The larger *c*-LP of $Nb_4C_3T_x$ is due to the higher water content between MXene layers.[38] The nature of intercalation between the nitride layers is not clear at this stage. The (002) peak of delaminated $Ti_4N_3T_x$ is also quite broad (Fig. 1a), which can be due to poor alignment of the small MXene flakes in the dry film. Two broad peaks at 28° and 36° were also observed (arrows in Fig. 1a), which possibly belong to rutile (TiO_2),[39] which is typically present as a result of delamination in TBAOH and DI water. This can also possibly be due to the slow oxidation of $Ti_4N_3T_x$ in aqueous solutions.[40]

Evidence of etching the Ti_4AlN_3 to form Ti_4N_3 was also provided by scanning electron microscopy (SEM) (Fig. 1b), which showed typical accordion-like structures. The latter, with clearly visible open layering, in a single particle, are characteristic of selective etching, in general[41] and HF etched MXenes in particular.[10] Energy-dispersive X-ray spectroscopy (EDX) of

the product, at low magnification, indicated that Al was still detected in a Ti : Al ratio of 4.0 : 0.9, which is similar to the starting Ti_4AlN_3, however, based on the XRD result (Fig. 1a), this could be attributed to Al-containing fluorides.

The delaminated $Ti_4N_3T_x$ particles were small, in the range of a few hundred nm (Fig. S2 in the ESI†). In a few cases, much larger flakes of about 1 μm in lateral size were observed as shown in Fig. 1c, which were more than a few layers thick, since they were not transparent to the 5 kV electron beam in SEM. Solutions of delaminated Ti_4N_3 flakes in DI water exhibit the Tyndall effect, shown by shining a laser beam through the solution (the inset in Fig. 1c), thereby confirming that this was a colloidal solution.

Furthermore, small $Ti_4N_3T_x$ flakes – with morphologies typical of other MXene flakes[12,38] – were observed in TEM micrographs (Fig. 2a and b). EDX determined these flakes to have no Al, thus confirming the formation of $Ti_4N_3T_x$. Selected-area electron diffraction (SAED) (top inset in Fig. 2b) of these $Ti_4N_3T_x$ flakes viewed normal to the basal (002) plane confirms their single-crystal nature, and the fact that the hexagonal symmetry ($P6_3/mmc$) of the parent MAX phase after exfoliation is retained. The *a*-LP of this flake from SAED is measured to be ~2.9 Å, which is similar to that of the Ti_4AlN_3 precursor,[32] indicating that, like all other MXenes synthesized to date, removing Al did not alter the in-plane structure of the nitride layers.

The Raman spectra of the untreated Ti_4AlN_3 and molten salt treated/acid washed Ti_4AlN_3 are shown in Fig. 2c. The Raman spectrum of the former is generally similar in terms of the peak positions previously reported.[42] The observed oscillation modes of certain symmetry groups of Ti_4AlN_3 are hence labeled after fitting the spectra with products of Gaussian and Lorentzian functions. Certain differences therein among the corresponding intensities of certain peaks could be due to the variations of vacancies and defects in the different samples analyzed. Moving forward, ω_2 (134.6 cm^{-1}), ω_5 (237.1 cm^{-1}) and ω_{10} (595.5 cm^{-1}) are E_{1g} group (irreducible representation) vibrations, which contain in-plane (shear) modes of Ti and N atoms. These peaks should remain present in the $Ti_4N_3T_x$ spectrum after etching Al from Ti_4AlN_3, but they decline in intensity and broaden presumably due to the increased interlayer spacing of the MXene structure, as can be seen in the bottom pattern of Fig. 2c. This change in the Raman spectra can be understood by visualizing parallels with the behavior of other 2D materials, such as the G-band of bilayer graphene, analogous to MXene, compared to that of few-layer graphene, analogous to the MAX phase.[43] The ω_4 (212.5 cm^{-1}), ω_7 (378.1 cm^{-1}), and ω_8 (548.5 cm^{-1}) modes are A_{1g} symmetry out-of-plane vibrations of Ti and N atoms. Therefore, if the Al interlayer is removed, the peaks of these vibrations are expected to red-shift, broaden and change their shape (Fig. 2c), analogous to the 2D-band of few-layered graphene *versus* that of bilayer graphene.[44]

The E_{2g} modes ω_3 (184.2 cm^{-1}) and ω_9 (558.6 cm^{-1}) are in-plane oscillations of Ti and N atoms, coupled to the minor oscillations of Al atoms. After etching, the Al atoms are exchanged with lighter atoms (such as H, F or O). Therefore, the intensities of such coupled oscillations are suppressed more than those of the E_{1g} oscillations mentioned. The broadening of these peaks in the Raman spectrum of $Ti_4N_3T_x$ could occur because of the increased disorder of the structure upon introduction of various surface moieties during etching, as well as decreased interlayer spacing. These features are present in the $Ti_4N_3T_x$ spectrum, indicating the removal of the Al layer. The in-plane E_{2g} symmetry mode ω_6 (251.2 cm^{-1}) is present in the Ti_4AlN_3 spectrum in Fig. 2c, diverse from the case of the corresponding Raman spectrum previously reported.[42] The energy of this mode, which consists of small oscillations of Ti and N atoms coupled to high-amplitude oscillations of Al, can be largely attributed to the latter. Elimination of Al would thus have the most impact on this peak. Indeed, diminishing of this peak evident in Fig. 2c confirms the successful removal of Al layers. It is important to note here that the Raman spectra of some spots in the acid washed molten salt treated Ti_4AlN_3 were similar to that of the non-treated Ti_4AlN_3 and are not shown here. This is in agreement with the XRD results (Fig. S1†), suggesting that non-etched Ti_4AlN_3 particles coexist with $Ti_4N_3T_x$ after the molten salt treatment.

To study the structure and electronic properties of non-terminated Ti_4N_3 and terminated $Ti_4N_3T_x$ (T = F, O, and OH) monolayers, we carried out spin-polarized density functional

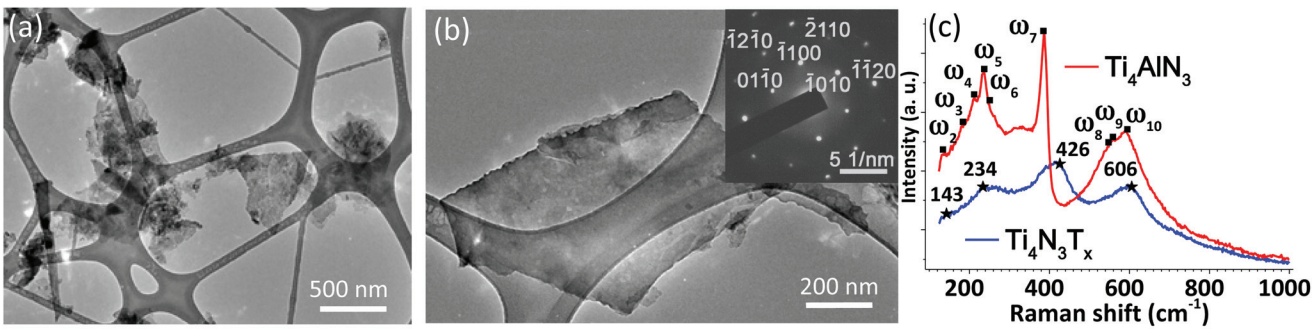

Fig. 2 TEM micrograph of (a) several delaminated flakes and (b) an individual $Ti_4N_3T_x$ flake. The inset in (b) shows the SAED pattern of the $Ti_4N_3T_x$ flake showing the hexagonal basal plane symmetry of the parent MAX phase. (c) Raman spectra of Ti_4AlN_3 (red curve) and delaminated $Ti_4N_3T_x$ (blue curve), with corresponding vibrational peaks found by fitting with a product of Gaussian and Lorentzian functions.

theory (DFT) calculations using the Vienna *ab initio* Simulation Package (VASP).[45,46] Details of the DFT calculations are further explained in the ESI.† Monolayer Ti_4N_3 was constructed from a MAX phase with a calculated lattice parameter a = 2.9915 Å and a thickness of L = 7.44 Å as shown in Fig. 3a. This result agrees well with the measured a-LP from the SAED pattern (Fig. 2b) and the previously predicted lattice parameters using the Perdew–Burke–Ernzerhof (PBE) method (a = 2.9929 Å).[32] The a-LPs of terminated $Ti_4N_3T_x$ were set equal to those of non-terminated Ti_4N_3, where the error in the lattice parameter is less than 0.03 Å.[36] We first evaluated the relative stability of the fully terminated Ti_4N_3 monolayers with different arrangements of surface terminations (F, O, and OH). Two energetically favorable arrangements of the surface terminations are considered, A and B, shown in Fig. 3b and c. Fig. 3(d–f) illustrates three possible arrangements of the surface terminations, namely AA, AB, and BB, in the fully terminated $Ti_4N_3T_x$ monolayers. The total energy differences with respect to configuration AA are listed in Table 1. Our calculations indicate that configuration AA (Fig. 3d) has the lowest energy for the F and O terminations, whereas for OH, the AB configuration (Fig. 3e) is more stable. This result is consistent with the previous DFT results for $Ti_4N_3T_x$.[36] In the case of carbide MXenes, configuration AA has been shown both experimentally and theoretically to be the most stable configuration.[36,47,48]

We then evaluated the formation energies of different surface terminations in order to predict which surface termination is more energetically preferred. In our case:

$$E_{\text{form}}(T) = \{E_{\text{tot}}(\text{Ti}_4\text{N}_3\text{T}_x) - E(\text{Ti}_4\text{N}_3) - xE(T)\}/x$$

where $E_{\text{form}}(T)$, $E_{\text{tot}}(\text{Ti}_4\text{N}_3\text{T}_x)$, $E(\text{Ti}_4\text{N}_3)$, and $E(T)$ are the formation energies of the termination group, the total energies of the terminated $Ti_4N_3T_x$ monolayers, non-terminated Ti_4N_3 monolayers, and surface termination groups (–F, –O, and –OH) calculated from VASP, respectively. The formation energies of

Table 1 Relative stability of functionalized $Ti_4N_3T_x$ with different arrangements of surface terminations, where the most stable configuration is in the bold font. Formation energies of –F, –O, and –OH surface terminations with single-side and double-side covered $Ti_4N_3T_x$ MXene. Calculated magnetic moment per unit cell for $Ti_4N_3T_x$ MXene. Note in all cases x = 2

		Ti_4N_3	$Ti_4N_3F_x$	$Ti_4N_3O_x$	$Ti_4N_3(OH)_x$
E–E_0 (eV)		AA	**0.000**	**0.000**	0.000
		AB	0.085	0.5284	**−0.012**
		BB	0.159	1.046	0.010
E_{form} (eV)	Single (Ti_4N_3T)	N/A	−5.804	−7.855	−5.332
	Double($Ti_4N_3T_2$)	N/A	−5.781	−7.773	−5.347
Magnetic moment per unit cell (μB)		7.00	0.88	0.37	0.00

single-sided and double-sided terminated $Ti_4N_3T_x$ monolayers are listed in Table 1. Based on these results we conclude that O terminations are energetically preferred compared to F and OH functional groups, while the OH termination is the least favorable one (even compared to F) with an energy difference of more than 0.4 eV per unit cell.

In order to shed light on the electronic properties of $Ti_4N_3T_x$, we calculated the spin-polarized partial density of states (PDOS) of the most stable configurations considering the contribution of different orbitals as shown in Fig. 4. For the $Ti_4N_3T_x$ and Ti_4N_3 monolayers, the main contribution near the Fermi level comes from the Ti 3d orbital, while a hybridization between the Ti 3d orbital and the N 2p orbital occurs from −2.0 to −8.0 eV below the Fermi level. The calculated total DOS at the Fermi level of bare, F-, O-, and OH-terminated Ti_4N_3 monolayers are 4.62, 4.0, 3.8, and 1.9 eV per unit cell respectively. This result indicates that the Ti_4N_3 monolayers are more metallic while the terminations lower the DOS at the Fermi level, similar to carbide MXenes.[36] On the other hand, the low DOS at the Fermi level of the OH terminated $Ti_4N_3T_x$ monolayer partially explains why OH is not energetically favor-

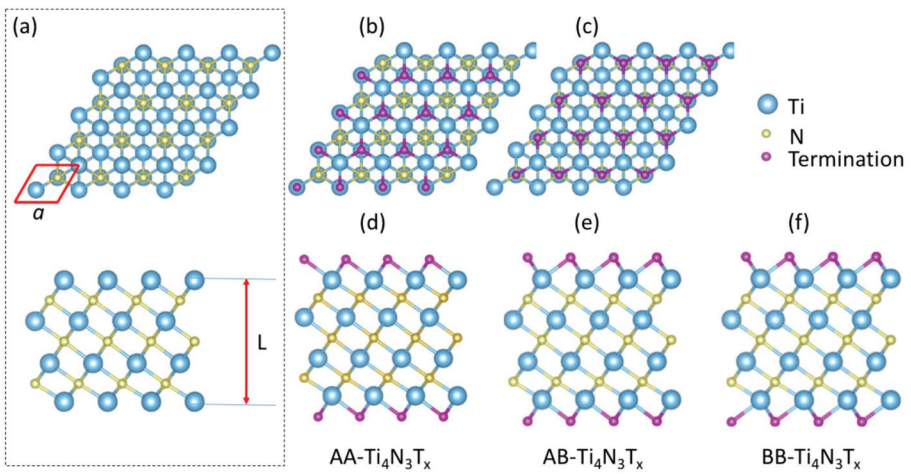

Fig. 3 (a) Crystal structure of Ti_4N_3 monolayers (top and side views are shown). For the single-sided terminations, two energetically favorable arrangements of the surface terminations are considered: (b) hollow site of surface Ti denoted by A, and (b) atop site of carbon denoted by B. In the case of double-sided terminations, the possible configurations of terminations are (d) AA-$Ti_4N_3T_x$, (e) AB-$Ti_4N_3T_x$, and (f) BB-$Ti_4N_3T_x$.

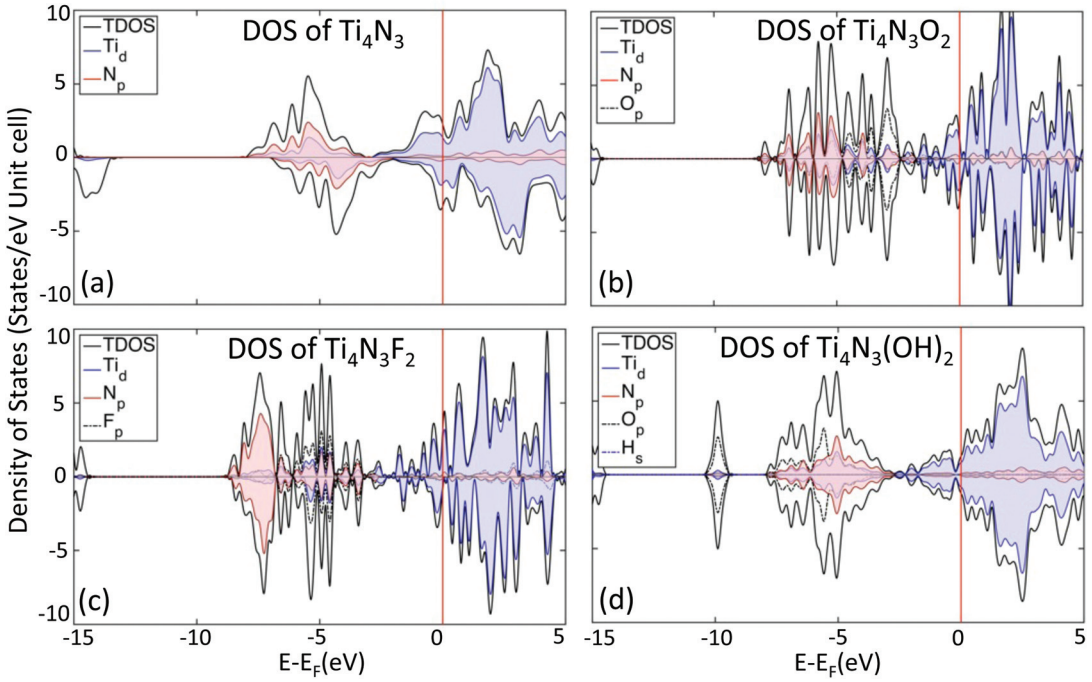

Fig. 4 Spin-polarized partial density of states of Ti_4N_3 monolayers and surface terminated $Ti_4N_3T_x$. The Fermi levels are set to zero and are indicated by the red line. TDOS refers to total density of states.

able. Note that previous studies[32,36] have only discussed the non-spin-polarized PDOS of the F terminated $Ti_4N_3T_x$ case, while here we are reporting a spin-polarized study on all possible terminations in $Ti_4N_3T_x$ (T = F, O, and OH). In Fig. 4, a magnetic moment of 7.0 μB per unit cell is predicted for bare Ti_4N_3, which results mainly from the unoccupied 3d orbitals of the Ti atoms. Surface terminations such as OH dramatically lower the magnetic moment to zero. These results differ from the previously reported DFT results which found that while a magnetic moment exists for the bare $Ti_{n+1}N_n$, functionalization with O, F, H, or OH groups reduces the magnetic moment to zero.[36]

In summary, we synthesized the first nitride MXene, two-dimensional titanium nitride, $Ti_4N_3T_x$. This was achieved by heating Ti_4AlN_3 in a molten fluoride salt, a method that has not been previously reported to produce MXenes from their corresponding MAX phases. Delamination of multilayered $Ti_4N_3T_x$ particles into few and monolayers was also achieved. DFT calculations of simulated $Ti_4N_3T_x$ determined that O terminations on $Ti_4N_3T_x$ (T = O) are the most energetically favorable compared to F and OH functional groups, while the OH termination is the least favorable. Relative to these terminated $Ti_4N_3T_x$ simulations, bare, non-terminated Ti_4N_3 is calculated to have the highest density of states, as well as a magnetic moment of 7.0 μB per unit cell.

Acknowledgements

This work was supported by the U.S. National Science Foundation under grant number DMR-1310245.

Notes and references

1 K. S. Novoselov, A. K. Geim, S. V. Morozov, D. Jiang, Y. Zhang, S. V. Dubonos, I. V. Grigorieva and A. A. Firsov, *Science*, 2004, **306**, 666–669.
2 J. N. Coleman, M. Lotya, A. O'Neill, S. D. Bergin, P. J. King, U. Khan, K. Young, A. Gaucher, S. De, R. J. Smith, I. V. Shvets, S. K. Arora, G. Stanton, H. Y. Kim, K. Lee, G. T. Kim, G. S. Duesberg, T. Hallam, J. J. Boland, J. J. Wang, J. F. Donegan, J. C. Grunlan, G. Moriarty, A. Shmeliov, R. J. Nicholls, J. M. Perkins, E. M. Grieveson, K. Theuwissen, D. W. McComb, P. D. Nellist and V. Nicolosi, *Science*, 2011, **331**, 568–571.
3 K. S. Novoselov, D. Jiang, F. Schedin, T. J. Booth, V. V. Khotkevich, S. V. Morozov and A. K. Geim, *Proc. Natl. Acad. Sci. U. S. A.*, 2005, **102**, 10451–10453.
4 R. Ma and T. Sasaki, *Adv. Mater.*, 2010, **22**, 5082–5104.
5 X. Zhang, J. Lei, D. Wu, X. Zhao, Y. Jing and Z. Zhou, *J. Mater. Chem. A*, 2016, **4**, 4871–4876.
6 X. Zhang, X. Zhao, D. Wu, Y. Jing and Z. Zhou, *Nanoscale*, 2015, **7**, 16020–16025.
7 X. Zhang, Z. Ma, X. Zhao, Q. Tang and Z. Zhou, *J. Mater. Chem. A*, 2015, **3**, 4960–4966.
8 Q. Tang, Z. Zhou and Z. Chen, *Wiley Interdiscip. Rev.: Comput. Mol. Sci.*, 2015, **5**, 360–379.
9 Y. Jing, Z. Zhou, C. R. Cabrera and Z. Chen, *J. Mater. Chem. A*, 2014, **2**, 12104–12122.
10 M. Naguib, M. Kurtoglu, V. Presser, J. Lu, J. Niu, M. Heon, L. Hultman, Y. Gogotsi and M. W. Barsoum, *Adv. Mater.*, 2011, **23**, 4248–4253.

11 M. Naguib and Y. Gogotsi, *Acc. Chem. Res.*, 2015, **48**, 128–135.
12 M. Naguib, J. Halim, J. Lu, K. M. Cook, L. Hultman, Y. Gogotsi and M. W. Barsoum, *J. Am. Chem. Soc.*, 2013, **135**, 15966–15969.
13 M. Naguib, O. Mashtalir, J. Carle, V. Presser, J. Lu, L. Hultman, Y. Gogotsi and M. W. Barsoum, *ACS Nano*, 2012, **6**, 1322–1331.
14 M. Naguib, V. N. Mochalin, M. W. Barsoum and Y. Gogotsi, *Adv. Mater.*, 2014, **26**, 992–1005.
15 M. W. Barsoum, in *MAX Phases*, Wiley-VCH Verlag GmbH & Co. KGaA, 2013, pp. 1–12.
16 B. Anasori, M. Dahlqvist, J. Halim, E. J. Moon, J. Lu, B. C. Hosler, E. A. N. Caspi, S. J. May, L. Hultman, P. Eklund, J. Rosén and M. W. Barsoum, *J. Appl. Phys.*, 2015, **118**, 094304.
17 J.-C. Lei, X. Zhang and Z. Zhou, *Front. Phys.*, 2015, **10**, 276–286.
18 M. W. Barsoum, *Prog. Solid State Chem.*, 2000, **28**, 201–281.
19 Z. Sun, D. Music, R. Ahuja, S. Li and J. M. Schneider, *Phys. Rev. B: Condens. Matter*, 2004, **70**, 092102.
20 M. Ghidiu, M. R. Lukatskaya, M.-Q. Zhao, Y. Gogotsi and M. W. Barsoum, *Nature*, 2014, **516**, 78–81.
21 J. Halim, M. R. Lukatskaya, K. M. Cook, J. Lu, C. R. Smith, L.-Å. Näslund, S. J. May, L. Hultman, Y. Gogotsi, P. Eklund and M. W. Barsoum, *Chem. Mater.*, 2014, **26**, 2374–2381.
22 B. Anasori, Y. Xie, M. Beidaghi, J. Lu, B. C. Hosler, L. Hultman, P. R. C. Kent, Y. Gogotsi and M. W. Barsoum, *ACS Nano*, 2015, **9**, 9507–9516.
23 M. W. Barsoum, J. Golczewski, H. J. Seifert and F. Aldinger, *J. Alloys Compd.*, 2002, **340**, 173–179.
24 T. El-Raghy, M. W. Barsoum and M. Sika, *Mater. Sci. Eng. A*, 2001, **298**, 174–178.
25 M. W. Barsoum, T. El-Raghy, L. Farber, M. Amer, R. Christini and A. Adams, *J. Electrochem. Soc.*, 1999, **146**, 3919–3923.
26 M. Naguib, V. Presser, N. Lane, D. Tallman, Y. Gogotsi, J. Lu, L. Hultman and M. W. Barsoum, *RSC Adv.*, 2011, **1**, 1493–1499.
27 M. Naguib, V. Presser, D. Tallman, J. Lu, L. Hultman, Y. Gogotsi and M. W. Barsoum, *J. Am. Ceram. Soc.*, 2011, **94**, 4556–4561.
28 Q. Ye, P. Xiao, W. Liu, K. Chen, T. Chen, J. Xue, S. Du and Q. Huang, *RSC Adv.*, 2015, **5**, 70339–70344.
29 M. N. Abdelmalak, *MXenes: A New Family of Two-Dimensional Materials and its Application as Electrodes for Li-ion Batteries*, PhD thesis, Drexel University, 2014.
30 R. Meshkian, L.-Å. Näslund, J. Halim, J. Lu, M. W. Barsoum and J. Rosen, *Scr. Mater.*, 2015, **108**, 147–150.
31 J. Zhou, X. Zha, F. Y. Chen, Q. Ye, P. Eklund, S. Du and Q. Huang, *Angew. Chem., Int. Ed.*, 2016, **55**, 5008.
32 I. R. Shein and A. L. Ivanovskii, *Comput. Mater. Sci.*, 2012, **65**, 104–114.
33 Y. Zhong, X. Xia, F. Shi, J. Zhan, J. Tu and H. J. Fan, *Adv. Sci.*, 2016, **3**, DOI: 10.1002/advs.201500286.
34 A. Morel, Y. Borjon-Piron, R. L. Porto, T. Brousse and D. Bélanger, *J. Electrochem. Soc.*, 2016, **163**, A1077–A1082.
35 G. V. Naik, J. L. Schroeder, X. Ni, A. V. Kildishev, T. D. Sands and A. Boltasseva, *Opt. Mater. Express*, 2012, **2**, 478–489.
36 Y. Xie and P. R. C. Kent, *Phys. Rev. B: Condens. Matter*, 2013, **87**, 235441.
37 M. Naguib, R. R. Unocic, B. L. Armstrong and J. Nanda, *Dalton Trans.*, 2015, **44**, 9353–9358.
38 M. Ghidiu, M. Naguib, C. Shi, O. Mashtalir, L. M. Pan, B. Zhang, J. Yang, Y. Gogotsi, S. J. Billinge and M. W. Barsoum, *Chem. Commun.*, 2014, **50**, 9517–9520.
39 J. Sun, L. Gao and Q. Zhang, *J. Am. Ceram. Soc.*, 2003, **86**, 1677–1682.
40 O. Mashtalir, K. M. Cook, V. N. Mochalin, M. Crowe, M. W. Barsoum and Y. Gogotsi, *J. Mater. Chem. A*, 2014, **2**, 14334–14338.
41 G. Z. Cambaz, G. N. Yushin, Y. Gogotsi and V. G. Lutsenko, *Nano Lett.*, 2006, **6**, 548–551.
42 N. J. Lane, M. Naguib, V. Presser, G. Hug, L. Hultman and M. W. Barsoum, *J. Raman Spectrosc.*, 2012, **43**, 954–958.
43 A. C. Ferrari and D. M. Basko, *Nat. Nanotechnol.*, 2013, **8**, 235–246.
44 A. C. Ferrari, J. C. Meyer, V. Scardaci, C. Casiraghi, M. Lazzeri, F. Mauri, S. Piscanec, D. Jiang, K. S. Novoselov, S. Roth and A. K. Geim, *Phys. Rev. Lett.*, 2006, **97**, 187401.
45 G. Kresse and J. Furthmüller, *Phys. Rev. B: Condens. Matter*, 1996, **54**, 11169–11186.
46 G. Kresse and J. Hafner, *Phys. Rev. B: Condens. Matter*, 1993, **47**, 558–561.
47 Q. Tang, Z. Zhou and P. Shen, *J. Am. Chem. Soc.*, 2012, **134**, 16909–16916.
48 H.-W. Wang, M. Naguib, K. Page, D. J. Wesolowski and Y. Gogotsi, *Chem. Mater.*, 2016, **28**, 349–359.